33rd Annual International Conference of the IEEE EMBS
Boston, Massachusetts USA, August 30 - September 3, 2011

CMOS Integrated Avalanche Photodiodes and Frequency-Mixing Optical Sensor Front End for Portable NIR Spectroscopy Instruments

Ruida Yun, Chirag Sthalekar and Valencia M. Joyner
Department of Electrical and Computer Engineering, Tufts University, Medford, MA, 02155
E-mail: ruida.yun@tufts.edu, chirag.sthalekar@tufts.edu, vjoyner@ece.tufts.edu

***Abstract*—This paper presents the design and measurement results of two avalanche photodiode structures (APDs) and a novel frequency-mixing transimpedance amplifier (TIA), which are key building blocks towards a monolithically integrated optical sensor front end for near-infrared (NIR) spectroscopy applications. Two different APD structures are fabricated in an unmodified $0.18\,\mu m$ CMOS process, one with a shallow trench isolation (STI) guard ring and the other with a P-well guard ring. The APDs are characterized in linear mode. The STI bounded APD demonstrates better performance and exhibits $3.78\,A/W$ responsivity at a wavelength of $690\,nm$ and bias voltage of $10.55\,V$. The frequency-mixing TIA (FM-TIA) employs a T-feedback network incorporating gate-controlled transistors for resistance modulation, enabling the simultaneous down-conversion and amplification of the high frequency modulated photodiode (PD) current. The TIA achieves $92\,dB\Omega$ conversion gain with $0.5\,V$ modulating voltage. The measured IIP_3 is $10.6\,\mu A$. The amplifier together with the $50\,\Omega$ output buffer draws $23\,mA$ from a $1.8\,V$ power supply.**

I. Introduction

NIR Spectroscopy (NIRS) is rapidly evolving as a promising non-invasive technique for functional imaging of the breast tissue, brain tissue, and skeletal muscle. The non-invasive nature of NIRS instruments has further found application in neonatal and fetal studies for long term monitoring of brain activity. Recent studies have shown an increased ability to predict and classify epileptic disturbances in children and neonates based on the simultaneous measurement of optical and electrical parameters using NIRS and EEG instruments[1]. Frequency-domain NIRS (FD-NIRS) techniques, employing sinusoidally-modulated excitation light, allow explicit separation of tissue absorption and scattering coefficients enabling further characterization of the physiological state of tissue. These wavelength-dependent optical parameters can provide information about the concentration of important biological chromophores, including hemoglobin, water, fat, NIR-absorbing drugs, and the composition, density, and organization of biological tissue structures (cells, organelles).

Fully exploiting the benefits of NIRS techniques demands a miniaturized instrument which is portable, unobtrusive, low-cost, low-power, and robust to motion artifacts. Advanced silicon microfabrication processing, such as CMOS technology, enables monolithic integration of photodetectors and electronic signal conditioning circuitry on a single substrate. Such high levels of integration make it possible to realize the entire NIRS receiver subsystem on a small chip[2], [3]. This offers several performance advantages by drastically reducing measurement noise and enabling realization of dense arrays of sensors to increase spatial mapping and detection at multiple tissue sites to enhance diagnostic capabilities.

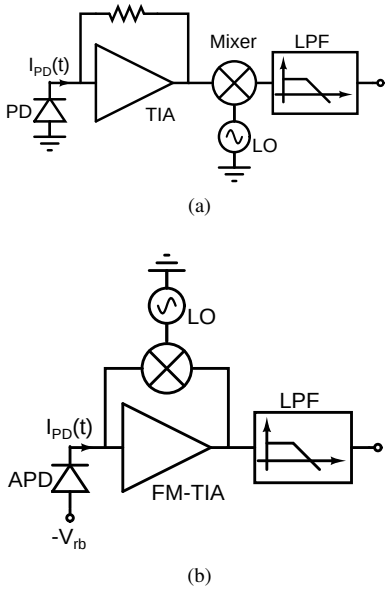

Figure 1: Schematic of the mixer based CMOS front-ends for NIRS. (a) traditional approach (b) frequency-mixing TIA with APD.

Fig. 1a depicts the schematic of a traditional mixer-based CMOS front end for FD-NIRS[3], where the wideband TIA amplifies the PD current and produces a voltage at the output. The subsequent mixer stage demodulates the signal and enables amplitude and phase detection. The commonly used N-well/P-sub PD offers very low responsivity and hence limits the sensitivity of the front end[2]. The excessive circuit noise from the wideband TIA further degrades performance. Furthermore, the mixer stage increases the complexity of the front end design and increases power consumption, especially for frequency-domain NIRS systems operating at a modulation frequency around $100\,MHz$.

This paper presents the design and measurement results of two CMOS APDs and a novel FM-TIA, which would signif-

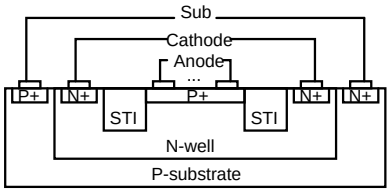

(a)

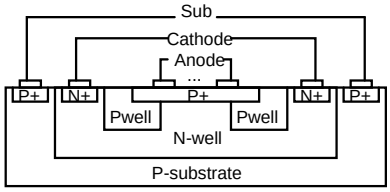

(b)

Figure 2: Cross-sectional view of APDs with guard ring in $0.18\,\mu m$ CMOS process (Not to scale). (a) APD with STI guard ring, (b) APD with P-well guard ring.

icantly improve the sensitivity of the optical sensor front end for NIRS instruments. The FM-TIA also simplifies the design by combining current-to-voltage conversion and demodulation of the received PD current simultaneously, enabling a compact and low power design with good linearity.

II. CMOS Avalanche Photodiode

CMOS APDs offer much higher responsivity compared to conventional PN diode structures because of the built-in multiplication gain, which is strongly dependent on its reverse bias voltage. However, the reverse bias voltage is limited by the breakdown voltage. If the APD is biased beyond its breakdown voltage, it operates in Geiger mode and is typically used with quenching circuitry for single photon counting. When biased slightly below the breakdown voltage, the APD works in linear mode and can be used for amplitude and phase detection. Hence it is necessary to increase the breakdown voltage of CMOS APD to improve its multiplication gain without driving it into avalanche breakdown.

Peripheral breakdown, typically found around the lateral edge of the junction, occurs earlier than the main P+/N-well junction breakdown and thus results in lower breakdown voltages[4]. Guard rings can be used to surround the junction and mitigate this premature breakdown. STI [5] and P-well[6] structures are the two types of guard rings available in a standard $0.18\,\mu m$ CMOS process as shown in Fig.2. The silicide layer is blocked to form an optical window for the STI-bounded APD, while the process prohibits such an optical window for the P-well bounded APD. Both types of CMOS APDs are implemented to study their performance.

III. Frequency-Mixing TIA

Fig.3 represents a FM-TIA with a fully differential topology, which is preferred to suppress higher order non-linearity and reject power supply noise. The frequency-mixing behavior of the proposed TIA can be understood by studying the half-circuit of the T-feedback network. If the transistor M_1 in

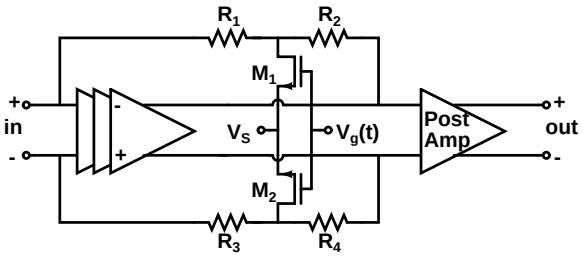

Figure 3: Schematic of the fully differential FM-TIA.

the T-feedback network is biased in deep triode region and its gate-to-source voltage is modulated by $V_{gs}(t) = V_{GS} + V_A\cos(2\pi f_{LO}t)$, its output conductance (g_{ds1}) is linearly proportional to $V_{gs}(t)$, such that the T-network equivalent feedback resistance R_F is modulated and given by

$$R_F(t) \approx R_2 + R_1(1 + g_{ds1}(t)\cdot R_2) \quad (1)$$

$$= R_{F0} + R_1R_2\beta V_A\cos(2\pi f_{LO}t) \quad (2)$$

Where the constant resistance R_{F0} is equal to $(1 + R_2\beta V_{OV})\,R_1 + R_2$, V_{OV} is the MOS transistor over-drive voltage and equals to $V_{GS} - V_{TH}$, β is the transconductance parameter. The time varying resistance $R_1R_2\beta V_A\cos(2\pi f_{LO}t)$ is mixed with a PD current for demodulation. Assuming that the received PD current is given by $I_{PD}(t) = I_A\cos(2\pi f_{RF}t)$, the feedback resistance $R_F(t)$ multiply with $I_{PD}(t)$ and generates three tones at $f_{RF} - f_{LO}$, f_{RF} and $f_{RF} + f_{LO}$. If the local oscillator (LO) frequency f_{LO} is close to the PD modulation frequency f_{RF}, then the generated three tones are well separated and the demodulated signal at $f_{RF} - f_{LO}$ can be easily selected by a Low Pass Filter (LPF).

The down-converted signal at the output can be expressed as

$$V_{out} = k_1I_A\cos\left(2\pi\left(f_{RF} - f_{LO}\right)t\right) \quad (3)$$

Where the conversion gain, k_1, can be defined as [7],

$$k_1 = \frac{1}{2}R_1R_2\beta V_A \quad (4)$$

However, the analysis so far is based on the first order approximation. Second order effects such as mobility degradation due to normal field have great impact on the conversion gain k_1. The effective transconductance parameter β_{eff} due to mobility degradation can be expressed as[8]

$$\beta_{eff} = \mu_0C_{ox}\frac{W}{L}\frac{V_{OV}}{1 + \theta_{mo}V_{OV}} \quad (5)$$

Where μ_0 denotes the low field mobility, θ_{mo} is the mobility degradation factor, C_{ox} is the gate oxide capacitance per unit area, W and L is the width and length of transistor M_1. The modulation voltage amplitude V_A has to be smaller than V_{OV} to keep M_1 always on and in the triode region. At the same time, V_A cannot be too high as a $V_{gs}(t)$ higher than V_{DD} will cause the gate oxide breakdown. So the maximum value of V_A

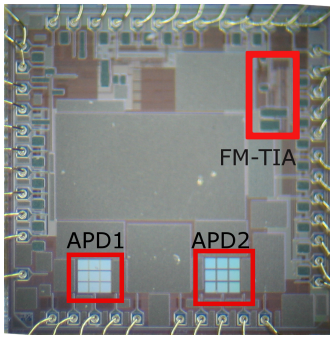

Figure 4: Microphotography of the test chip of CMOS APDs and FM-TIA, where APD1 is STI bounded and APD2 is P-Well bounded.

is achieved by biasing M_1 with $V_{OV,max} = (V_{DD} - V_{TH})/2$. It can be shown that a more accurate expression for k_1 can be expressed as

$$k_1 \approx \frac{1}{2}\frac{\mu_0 C_{ox}\frac{W}{L}R_1R_2}{(1+\theta_{mo}V_{OV})^2}V_A \leq \frac{1}{2}\frac{\mu_0 C_{ox}\frac{W}{L}R_1R_2}{(1+\theta_{mo}V_{OV})^2}V_{OV} \quad (6)$$

A three-stage core amplifier is employed and each gain stage has $18.6\,dB$ gain and $1.2\,GHz$ bandwidth to ensure circuit stability. A post amplifier is also implemented on-chip and incorporates a buffer stage to drive a $50\,\Omega$ off-chip load[7]. Transistors M_1/M_2 are identical in Fig.3 and are small dimension devices to minimize the parasitic capacitance at the transistor drain. Resistors R_1/R_3 are chosen to be $60k\Omega$ and R_2/R_4 are $1\,k\Omega$. The source voltage of M_1 is biased at $0.9\,V$ such that the drain-to-source voltage is $15\,mV$, for deep triode region operation. The d.c. gate voltage of M_{1-2} is set to $2.05\,V$ such that $V_{OV} = 0.6\,V$.

IV. Experimental Results

Two CMOS APDs and an FM-TIA are fabricated in a standard unmodified $0.18\,\mu m$ CMOS process. Fig. 4 show the microphotograph of the chip. Each of the APD consists of a 3×3 array of small photodiodes resulting in a total area of $0.3 \times 0.3, mm^2$. The active area of the amplifier is $0.70 \times 0.27 mm^2$. It draws $23\,mA$ current from a $1.8\,V$ supply voltage while driving $50\,\Omega$ loads. The core FM-TIA consumes only $6.6\,mA$ and the output buffer draws $16.4\,mA$ from the power supply.

The I-V characteristics of the two CMOS APDs (APD1 and APD2) are measured with and without illumination at room temperature shown in Fig.5a. The APD2 device (P-well bounded) exhibits $10.9\,V$ breakdown voltage, which is $300\,mV$ higher than the breakdown voltage of the STI-bounded structure. The dark current slowly increases at low reverse bias voltages, and then drastically changes to $1\,mA$ for bias voltages higher than the breakdown voltage. The APD1 device (STI bounded) exhibits lower dark current at low bias voltage. When both APDs are exposed to a $690\,nm$ laser diode and receive $235\,nW$ optical power, APD1 generates almost two times higher photocurrent than APD2, which indicates that the silicide layer on top of the P-Well attenuates the optical

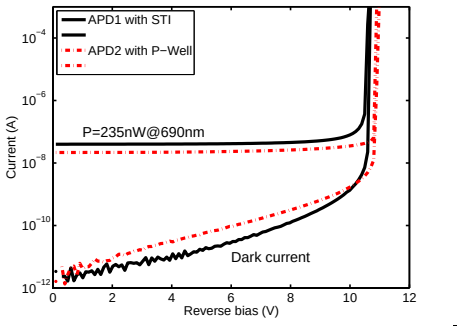

(a)

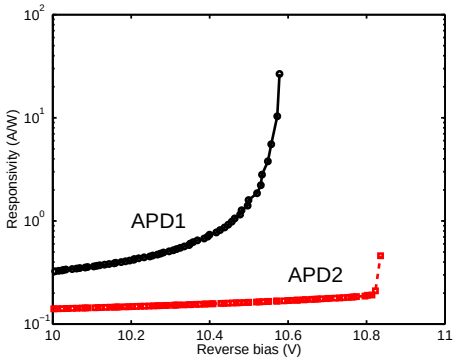

(b)

Figure 5: (a) Measured CMOS APD I-V characteristics, (b) Measured responsivity at $\lambda = 690\,nm$ against the bias voltage.

power significantly. Fig. 5b shows the measured responsivity at $690\,nm$ versus the bias voltage. The responsivity of APD1 gradually increases with bias voltage while the response of APD2 abruptly changes at higher bias voltages. The responsivity of the STI bounded structure (APD1) is significantly higher than APD1, but at the expense of higher dark current levels. The responsivity is approximately $3.78\,A/W$ for APD1 and the dark current is $15.5\,nA$ at a bias voltage of $50\,mV$ below the breakdown voltage. This responsivity can be improved to $10.34\,A/W$ with dark current levels reaching $30\,nA$ at a bias voltage of $30\,mV$ below the breakdown voltage.

Fig. 6 shows the measured capacitance per unit area versus bias voltage. It is clear that the high bias voltage around breakdown reduces the parasitic capacitance of APDs by more than $50\,\%$. The reduced parasitic capacitance of the APD compared to PN/PiN photodiodes biased at lower voltages with the same area is a clear advantage of this structure for high frequency operation.

APD emulation circuit is used to facilitate the electrical measurement of the proposed FM-TIA, where a $1\,k\Omega$ resistor converts the voltage signal into current signal and a $4\,pF$ capacitor is used to model the PD parasitic capacitance. The frequency-mixing capability of the proposed TIA is first examined by studying its output spectrum, where a $1.6\,\mu A$ photodiode current ($f_{RF} = 100\,MHz$) and a $0.5\,V$ local oscillator signal ($f_{LO} = 90\,MHz$) are fed to the FM-TIA. The result is shown in Fig.7, where the demodulated signal is clearly visible at $f_{IF} = 10\,MHz$ with $-26\,dBm$ power.

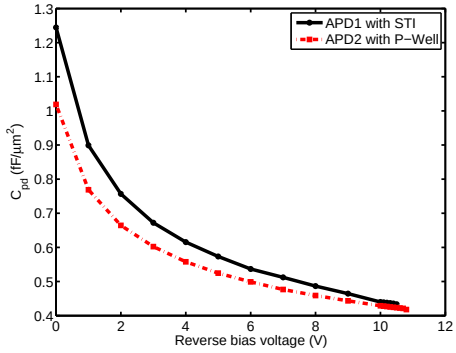

Figure 6: Measured CMOS APD C-V characteristics.

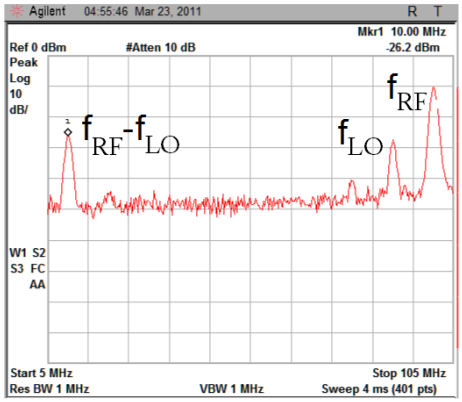

Figure 7: Frequency spectrum of FM-TIA output.

The conversion gain (k_1) is measured by sweeping the modulating voltage signal amplitude (V_A). Fig.8 demonstrates that k_1 is linearly proportional to V_A as expected, with maximum value of $39\,k\Omega$ when V_A is increased to $0.5\,V$. V_A is limited to $0.5\,V$ so that the transistor M_1/M_2 can safely operate in triode region.

The linearity of the FM-TIA is demonstrated with two-tone test. The IIP_3 is measured using PD current modulated with two tones at $100\,MHz$ and $99.5\,MHz$, and the LO frequency is set to $91\,MHz$ with $0.5\,V$ amplitude. As shown in Fig.9, the measured IIP_3 is $10.6\,\mu$A and the measured $1\,dB$

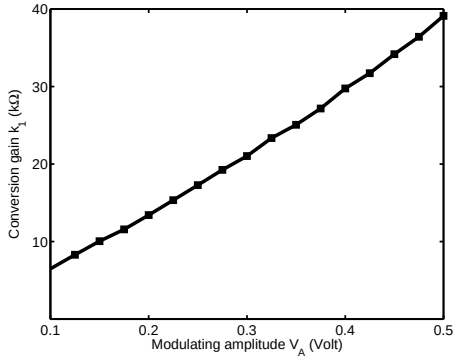

Figure 8: Measured conversion gain k_1 versus modulating voltage amplitude V_A, where $f_{RF} = 100\,MHz$, $f_{LO} = 99\,MHz$ and $f_{IF} = 1\,MHz$.

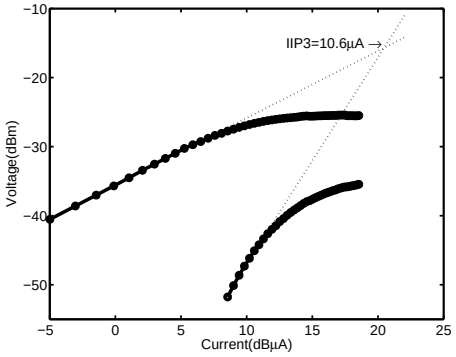

Figure 9: Measurement results of two-tone test.

compression point is $3.1\,\mu A$, which is roughly $10\,dB$ below IIP_3.

V. Conclusion

The design and measurement results of CMOS APDs and a novel FM-TIA are presented here. The STI bounded APD demonstrate $3.78\,A/W$ responsivity at $690\,nm$ with $10.55\,V$ bias voltage and the corresponding dark current is only $15.5\,nA$. The P-Well APD suffers from poor responsivity due to the opaque silicide layer on top of it. The novel FM-TIA, combining current-to-voltage amplification with frequency mixing, is capable of directly down-converting the RF-modulated PD generated current signal with high gain and good linearity. Measurement results reveal that the FM-TIA achieves $92\,dB\Omega$ current-to-voltage conversion gain. The measured IIP_3 point is $10.6\,\mu A$. The amplifier including $50\,\Omega$ output buffer draws $23\,mA$ from a $1.8\,V$ power supply.

References

[1] F. Wallois, A. Patil, C. Héberlé, and R. Grebe, "EEG-NIRS in epilepsy in children and neonates," *Neurophysiologie Clinique/Clinical Neurophysiology*, vol. 40, no. 5-6, pp. 281 – 292, 2010.

[2] R. Yun and V. M. Joyner, "A monolithically integrated phase-sensitive optical sensor for frequency-domain NIR spectroscopy," *IEEE Sensors Journal*, vol. 10, no. 7, pp. 1234–1242, 2010.

[3] F. Normandin, M. Sawan, and J. Faubert, "A new integrated front-end for a noninvasive brain imaging system based on near-infrared spectroreflectometry," *IEEE Transactions on Circuits and Systems I: Regular Papers*, vol. 52, no. 12, pp. 2663–2671, 2005.

[4] A. Rochas, A. R. Pauchard, P. A. Besse, D. Pantic, Z. Prijic, and R. S. Popovic, "Low-noise silicon avalanche photodiodes fabricated in conventional CMOS technologies," *IEEE Transactions on Electron Devices*, vol. 49, no. 3, pp. 387–394, March 2002.

[5] H. Finkelstein, M. J. Hsu, and S. C. Esener, "STI-bounded single-photon avalanche diode in a deep-submicrometer CMOS technology," *IEEE Electron Device Letters*, vol. 27, no. 11, pp. 887–889, Nov. 2006.

[6] M. A. Marwick and A. G. Andreou, "Fabrication and testing of single photon avalanche detectors in the TSMC 0.18um CMOS technology," in *Proc. 41st Annual Conference on Information Sciences and Systems CISS '07*, 14–16 March 2007, pp. 741–744.

[7] R. Yun and V. M. Joyner, "A CMOS frequency-mixing transimpedance amplifier with $5nA_{rms}$ input noise for frequency-domain near-infrared spectroscopy," in *Proc. IEEE Biomedical Circuits and Systems Conf. (BioCAS)*, 2010, pp. 238–241.

[8] Q. Huang, "A MOSFET-only continuous-time bandpass filter," *IEEE Journal of Solid-State Circuits*, vol. 32, no. 2, pp. 147–158, 1997.